Sensorless Control and On-line Estimation of Inductances of IPMSMs Using Current Derivatives

Minh Xuan Bui[1], Khac Thuy Le[1], Thanh Tien Nguyen[1], Dan Xiao[2], Faz Rahman[2], *IEEE Fellow*

[1]: Le Quy Don Technical University, Hanoi, Vietnam

[2]: University of New South Wales, Sydney, Australia

Abstract –This paper presents a sensorless control method and a very fast on-line estimation method of inductances of an IPMSM. The current derivatives at one active-voltage vector and one zero-voltage vector are measured every PWM cycle to estimate the rotor speed and position with the aim of increasing the estimation accuracy and reducing total harmonic distortion. In addition, machine inductances can be estimated on-line based on these current derivatives and the DC bus voltage of the inverter. The proposed on-line parameter identification method can overcome the drawback of the existing off-line methods, namely the requirement of a robust mechanical clamping system and test signal generators. The proposed on-line method also addresses the limit of the existing on-line methods, such as slow update and the possibility of incorrect convergence of the estimated parameters. Extensive experimental studies were conducted to verify the effectiveness and robustness of the proposed sensorless control and parameter identification of the IPMSM.

***Index Terms*—Sensorless Control, On-line Parameter Identification, Current Derivative Measurement**

I. INTRODUCTION

Sensorless control of permanent magnet synchronous motor have been developed significantly over the recent decades with the aim of reducing the size, cost and increase of reliability of the drive system. It is well-known that at low and zero speeds, the sensorless methods based on the saliency, such as signal injections take the advantages, while during medium and high speeds the sensorless methods based on the machine model are widely used. Combination of these two methods have been proposed where at low and very low speeds the signal injection methods are utilized, while at medium and high speeds the model-based methods are fully dominated. The signal injection-based methods lead to the increase of current torque ripple, acoustic noise and the power loss, while the model-based methods are sensitive to the accuracy of machine parameters and non-linearity of the inverter.

The methods based on the measurement of current derivatives at voltage vectors during PWM cycles are saliency-based methods, which can improve the bandwidth of the estimators. These methods include Indirect Flux Detection by Online Reactance Measurement (INFORM) [1], Extended Modulation [2] and Fundamental PWM Excitation (FPE) [3-7]. Of these methods, the FPE methods have the highest bandwidth up to PWM frequency. The conventional FPE sensorless methods are based on the measurement of current derivatives at two active- and two zero-voltage vectors in each standard PWM cycle.

Current derivatives can be measured by using the dedicated current derivative sensor (such as Rogowski coil) or estimated directly by sampling two current samples during a specific interval. Alternatively, current derivatives can be estimated more accurately by using the curve fitting algorithm based on a number of current samples. It is well-known that the common-mode noise, known as high frequency oscillation (HF) component of the phase current after switching transition, affects the accuracy of current sampling and current derivative calculation. Therefore, the sampling must be delayed after switching transition for certain duration until this common-mode noise die out. However, during the operation of the system, the voltage vector is sometimes shorter than this oscillation duration. As a result, this voltage vector must be extended to minimum duration of time (t_{min}) in order to guarantee the accuracy of current derivative estimation.

For SPMSMs with small inductances, the HF oscillation duration is less than about 8μs. Consequently, the extension of two active-voltage vectors and two zero-voltage vectors does not significantly affect the current waveform and the performance of the systems. However, for IPMSMs, which have much larger inductances, the oscillations of phase currents last about 20μs at full load operation. As a result, voltage vectors have to be extended far longer than for SPMSMs, which results in highly distorted stator currents. Therefore, this paper proposes a sensorless control method, which is based on the measurement of current derivatives at only one active-voltage vector and one zero-voltage vector during each PWM cycle with the aim of improving the estimation accuracy and reducing the current distortion over a full speed range from zero to rated speed, compared to the conventional FPE sensorless method.

It is worth noting that current derivative of each phase has a direct relationship with the machine inductances and the DC bus voltage of the inverter. Therefore, the machine inductances can be estimated directly by measuring current derivatives and the DC bus voltage. Since the current derivatives can be measured during a PWM cycle, the estimated inductance can be updated very fast at PWM frequency. This also facilitates a new on-line identification method of the machine inductances. This proposed on-line method can overcome the weakness of the existing off-line methods, namely the requirement of additional hardware and the spending of much time and effort to collect and process a huge amount of data [8-11]. The proposed on-line method requires no recursive algorithm and no signal injection, thus overcoming the drawbacks of the existing on-line methods, which are based on the machine's dynamic equations and the application of recursive algorithms, such as: Recursive Least Square (RLS) or Affine Projection Algorithm (APA) [12-14]. In general, these existing on-line methods take considerable time encompassing many PWM cycles, due to the recursive process, to achieve the convergence of the algorithm. In addition, tuning of the parameters of the RLS or APA is not straightforward. There is

978-1-7281-1249-7/19/$31.00 ©2019 IEEE

possibility of incorrect convergence of the estimated parameters. Furthermore, the injected signals cause current distortion and affect the general performance of the system.

Therefore, this paper also presents an on-line method for estimating the inductances of the IPMSM by measuring current derivatives and the DC bus voltage of the inverter every PWM cycle. Furthermore, the implementation issues regarding the estimation of current derivatives are presented. In addtion, the pulse stretching scheme and ripple analysis are described to demonstrate the advantages of the proposed sensorless control method. Extensive experimental studies were conducted to verify the effectiveness and robustness of the proposed sensorless control and parameters estimation methods.

II. SENSORLESS CONTROL AND INDUCTANCE ESTIMATION BASED ON CURRENT DERIVATIVE MEASUREMENT

A. Estimation of rotor speed and position

Scalars p_A, p_B, p_C of the position vector are defined as:

$$\begin{aligned} p_A &= \frac{2L_\Delta}{L_\Sigma + \frac{2}{3}L_\sigma}\cos(2\theta_e) \\ p_B &= \frac{2L_\Delta}{L_\Sigma + \frac{2}{3}L_\sigma}\cos(2\theta_e - 2\pi/3) \\ p_C &= \frac{2L_\Delta}{L_\Sigma + \frac{2}{3}L_\sigma}\cos(2\theta_e - 4\pi/3) \end{aligned} \tag{1}$$

where θ_e is the electrical angle of the rotor.

$$\begin{aligned} L_\Sigma &= \frac{L_d + L_q - 2L_\sigma}{3} \\ L_\Delta &= \frac{L_d - L_q}{3} \end{aligned} \tag{2}$$

where L_σ is the leakage inductance of stator winding; L_d, L_q are direct- and quadrature- axes inductances respectively.

The current derivatives at the longer active-voltage vector and at zero voltage-vector during the first half of each PWM cycle are measured to calculate the position scalar. The equation for calculating the position scalars are shown in Table I [15].

$$g = \frac{9}{2V_{DC}}(L_\Sigma + \frac{2}{3}L_\sigma)\left(1 - \left(\frac{L_\Delta}{L_\Sigma + \frac{2}{3}L_\sigma}\right)^2\right) \tag{3}$$

The quantity g in (3) is updated during operation and takes into account the change of L_{di} and L_{qi} (determined by L_Σ and L_Δ) as well as variation of the DC bus voltage (V_{DC}). The value of g is calculated by assuming that the rotor position is unchanged during two consecutive PWM cycles where there is a change of the selected active-voltage vector for current derivative measurement and positional scalar calculation as shown in Table II [15].

The scalars of the position vector in the stationary reference frame can be expressed as:

$$\begin{aligned} p_\alpha &= (2p_A - p_B - p_C)/3 = \frac{2L_\Delta}{L_\Sigma + \frac{2}{3}L_\sigma}\cos(2\theta_e) \\ p_\beta &= (p_B - p_C)/\sqrt{3} = -\frac{2L_\Delta}{L_\Sigma + \frac{2}{3}L_\sigma}\sin(2\theta_e) \end{aligned} \tag{4}$$

where p_α, p_β are the position scalars in the stationary reference frame.

The phase lock loop is then used to estimate rotor speed and position. The design details of this PLL is shown in [16].

TABLE I
POSITION SCALARS OF IPMSM WITH STAR CONNECTION

Active and zero-voltage vector	p_A	p_B	p_C
V_1 and V_0	$2-g\left(\frac{di_A^{(1)}}{dt}-\frac{di_A^{(0)}}{dt}\right)$	$-1-g\left(\frac{di_C^{(1)}}{dt}-\frac{di_C^{(0)}}{dt}\right)$	$-1-g\left(\frac{di_B^{(1)}}{dt}-\frac{di_B^{(0)}}{dt}\right)$
V_2 and V_0	$-1+g\left(\frac{di_B^{(2)}}{dt}-\frac{di_B^{(0)}}{dt}\right)$	$-1+g\left(\frac{di_A^{(2)}}{dt}-\frac{di_A^{(0)}}{dt}\right)$	$2+g\left(\frac{di_C^{(2)}}{dt}-\frac{di_C^{(0)}}{dt}\right)$
V_3 and V_0	$-1-g\left(\frac{di_C^{(3)}}{dt}-\frac{di_C^{(0)}}{dt}\right)$	$2-g\left(\frac{di_B^{(3)}}{dt}-\frac{di_B^{(0)}}{dt}\right)$	$-1-g\left(\frac{di_A^{(3)}}{dt}-\frac{di_A^{(0)}}{dt}\right)$
V_4 and V_0	$2+g\left(\frac{di_A^{(4)}}{dt}-\frac{di_A^{(0)}}{dt}\right)$	$-1+g\left(\frac{di_C^{(4)}}{dt}-\frac{di_C^{(0)}}{dt}\right)$	$-1+g\left(\frac{di_B^{(4)}}{dt}-\frac{di_B^{(0)}}{dt}\right)$
V_5 and V_0	$-1-g\left(\frac{di_B^{(5)}}{dt}-\frac{di_B^{(0)}}{dt}\right)$	$-1-g\left(\frac{di_A^{(5)}}{dt}-\frac{di_A^{(0)}}{dt}\right)$	$2-g\left(\frac{di_C^{(5)}}{dt}-\frac{di_C^{(0)}}{dt}\right)$
V_6 and V_0	$-1+g\left(\frac{di_C^{(6)}}{dt}-\frac{di_C^{(0)}}{dt}\right)$	$2+g\left(\frac{di_B^{(6)}}{dt}-\frac{di_B^{(0)}}{dt}\right)$	$-1+g\left(\frac{di_A^{(6)}}{dt}-\frac{di_A^{(0)}}{dt}\right)$

B. Estimation of machine inductances

Solving (3) and (4), the incremental inductances can be calculated as:

$$\begin{aligned} L_{qi} &= \frac{gV_{DC}}{3(1-\frac{\sqrt{p^2{}_\alpha + p^2{}_\beta}}{2})} \\ L_{di} &= \frac{gV_{DC}}{3(1+\frac{\sqrt{p^2{}_\alpha + p^2{}_\beta}}{2})} \end{aligned} \tag{5}$$

The apparent inductances are obtained by integrating the incremental inductance:

$$L_{d,q}^{(n)} = \frac{\Phi_{d,q}^{(n)}}{I_{d,q}^{(n)}} = \frac{\Sigma L_{di,qi}^{(k)}(I_{d,q}^{(k)} - I_{d,q}^{(k-1)})}{I_{d,q}^{(n)}}, k=1\text{-}n \tag{6}$$

where $\Phi_{d,q}^{(n)}$ are the total flux, $L_{d,q}^{(n)}$ are the apparent inductance, $L_{di,qi}^{(k)}$ are the incremental inductances calculated from (5), $I_{d,q}^{(k)}$ is the *d*- and -*q* current.

The discrete integration in (6) is carried out for *n* values of current levels from zero to the operating level, stored in an array. The value of *n* is determined by the acceptable resolution of integration and the operating current level. In this study, the incremental current change for each integration step is 0.1A.

It is noted that the update of quantity *g* in Table II determines how fast the estimated inductances are updated. By measuring the current derivatives two active- and one- zero voltage vectors during each PWM cycle, quantity *g* and the estimated inductances can be updated at switching frequency.

TABLE II
CALCULATION OF *g*

Active-voltage vectors	*g*
V_1 and V_2	$\frac{3}{\frac{di_A^{(1)}}{dt}-\frac{di_A^{(0)}}{dt}+\frac{di_B^{(2)}}{dt}-\frac{di_B^{(0)}}{dt}}$
V_2 and V_3	$\frac{3}{\frac{di_A^{(2)}}{dt}-\frac{di_A^{(0)}}{dt}+\frac{di_B^{(3)}}{dt}-\frac{di_B^{(0)}}{dt}}$
V_3 and V_4	$\frac{-3}{\frac{di_A^{(4)}}{dt}-\frac{di_A^{(0)}}{dt}+\frac{di_C^{(3)}}{dt}-\frac{di_C^{(0)}}{dt}}$
V_4 and V_5	$\frac{-3}{\frac{di_A^{(4)}}{dt}-\frac{di_A^{(0)}}{dt}+\frac{di_B^{(5)}}{dt}-\frac{di_B^{(0)}}{dt}}$
V_5 and V_6	$\frac{-3}{\frac{di_A^{(5)}}{dt}-\frac{di_A^{(0)}}{dt}+\frac{di_B^{(6)}}{dt}-\frac{di_B^{(0)}}{dt}}$
V_6 and V_1	$\frac{3}{\frac{di_A^{(1)}}{dt}-\frac{di_A^{(0)}}{dt}+\frac{di_C^{(6)}}{dt}-\frac{di_C^{(0)}}{dt}}$

C. Pulse stretching scheme and current ripple analysis

To tackle the parasitic effect on the di/dt measurement accuracy, the narrow voltage vector must be extended to the minimum pulse width (t_{min}), which is longer than the high-frequency oscillation time of the phase current. The extension of the narrow voltage vector changes fundamental PWM sequence, thus changing the final voltage vectors applied to the motor. These changes of voltage vector lead to additional current distortion, torque ripples and acoustic noise. The compensation of the extended voltage vector must be implemented in order to reduce these undesired effects. This compensation scheme should keep the duty cycles of three phases unchanged. For example, V_1 is required to be extended and compensated as shown in Fig. 1(a). The PWM pulse for phase A is shifted towards the beginning point of the PWM. The first half duration of V_0 becomes shorter than the second-half. However, the total lengths of V_1 and V_0 are kept the same.

In order to evaluate the effectiveness of the proposed stretching scheme, the comparative analysis of the ripples caused by the proposed FPE sensorless method and the conventional FPE sensorless method is implemented. In the proposed FPE method, only one active-voltage vector at the first half of a PWM cycle is selected to measure the current derivatives, while for the conventional FPE method two active-voltage vectors at the first half of a PWM cycle are selected to measure the current derivatives. For example, the stator voltage vector is modulated in sector I with two active-voltage vectors, V_1 and V_2. The duration of V_2 is longer than that of V_1 and both durations of V_1 and V_2 are smaller than t_{min}. For the conventional FPE method, both V_1 and V_2 are extended in one PWM cycle. In contrast, for the proposed method only the longer active voltage vector is extended (V_2 in this case). Following the technique presented in [17], the voltage ripple and current ripple waveforms for the extension and compensation of the voltage vector V_1 and V_2 are sketched in Fig. 1 (a) and (b) respectively.

It is worth noting that the *d- or q-* current ripple caused by the conventional FPE sensorless method is the sum of two corresponding shaded areas in Fig. 1(a) and (b), while the *d- or q-* current ripple caused by the proposed method is only one shaded area in Fig. 1(a) or (b). As a result, the current ripple of the proposed sensorless method is smaller than that of the conventional FPE sensorless method.

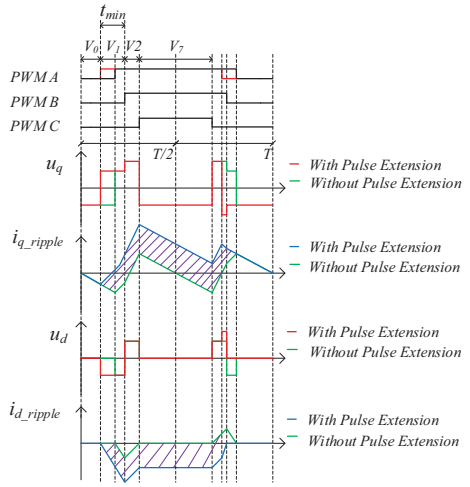

(a) Extension of V_1

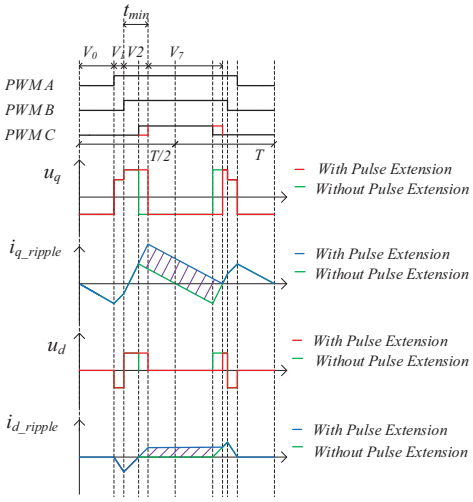

(b) Extension of V_2

Fig. 1. Voltage and current ripple during one PWM cycle.

III. EXPERIMENTAL SETUP

A. Experimental setup

As shown in Fig. 2, the experimental setup consists of one Field Programmable Gate Array (FPGA) board, one digital processor dSPACE1103, one ADC board with four channels and the resolution of 12bit, one 3-level voltage source inverter, one tested IPMSM coupled with one DC generator for loading, one H-bride for regulating the load current. The FPGA (ML605) is used to generate the PWM signals to the gate driver of the inverter, to calculate the current derivatives and to generate a clock for synchronizing the current sampling and current derivative calculation. dSPACE1103 is used to implement the Field Oriented Control (FOC) of the IPMSM, to calculate the machine inductances and to estimate rotor speed and position. The tested machine is a commercial Kollmorgan IPMSM, of which the parameters are shown in Table III. The Anisotropic Magnetoresistance (AMR) current sensors with bandwidth up to 2 MHz are used to sense the machine current for di/dt calculation and for the feedback of *d*- and *q*- axes current controllers.

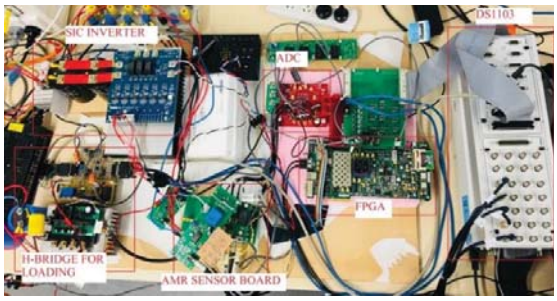

Fig. 2. Experimental setup.

TABLE III
PARAMETERS OF IPMSMS TESTED AND CONTROL SYSTEM

Number of pole pair	2
Stator resistance	5.8 Ω
Magnet flux linkage	0.533 Wb
d-axis inductance	0.0448 H
q-axis inductance	0.1024 H
Phase voltage (rms)	230 V
Phase current (rms)	3 A
Rated torque	6 Nm
Rated speed	1500 rpm
Switching frequency	5 kHz
Sampling rate of ADCs	50 MSPS
t_{min}	24 µs

B. Implementation issues on current derivative measurement

In order to mitigate the common-mode noise on the measurement of current derivatives, some methods have been proposed in [3]. In this study, in order to address the common-mode noise effect, high bandwidth current sensors (AMR sensor with the bandwidth of about 2 MHz) and high speed ADCs (50 MSPS) have been utilized to obtain a high number of current samples for di/dt calculation, which is based on the curve fitting Least Square Algorithm as following [18]:

$$\frac{di}{dt} = \frac{n\sum_{i=1}^{n} x_i y_i - \sum_{i=1}^{n} x_i \sum_{i=1}^{n} y_i}{n\sum_{i=1}^{n} x_i^2 - (\sum_{i=1}^{n} x_i)^2} \tag{7}$$

where x_i and y_i represent the time and the current sample respectively; n is the number of total samplings.

RC filter has been utilized in the customized AMR sensor boards in order to reduce the common-mode noise from current sensing. Moreover, the sampling of the current waveforms is delayed until the HF oscillations in current die out. The duration of high-frequency oscillation of the phase current after switching transition for the tested IPMSM (about 20 µs under full load) is far longer than that of the PMSM (about 8µs). Therefore, the sampling of the phase current is delayed by 20 µs after the switching transition. A minimum of pulse width (t_{min}) of 24 µs was implemented in order to obtain at least 200 current samples for *di/dt* calculation, which can guarantee the satisfactory accuracy of current derivative measurement.

IV. EXPERIMENTAL RESULTS

A. Current derivative estimation

Firstly, the oscilloscope is used to capture the machine current and the PWM signals. The sampling frequency of the oscilloscope is set to be 50 MHz. The voltage vectors during PWM cycles are determined by processing the PWM signals of three phases. The current derivatives are calculated in Matlab based on the current samples during each voltage vector and the application of the recursive least square and least square algorithms.

Fig. 3 compares the estimated current derivatives at the longer active-voltage vector during every PWM cycles, which are obtained by using recursive least square (RLS) and least square (LS) algorithms. The current samples used for di/dt calculation are delayed from the switching transition by 20 µs. It is clear that two methods result in the fairly similar current derivative estimation. However, the RLS algorithm takes longer time to obtain the current derivatives than the LS algorithm.

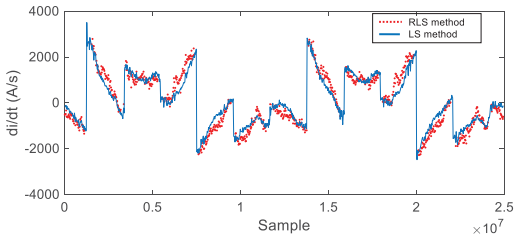

Fig. 3. Current derivative calculation at 300 rpm (experiment).

Fig. 4 compares the phase current derivatives at the first- and second- active-voltage vectors during each PWM cycle, which are obtained by simulation and experiment. The IPMSM is operated at 300 rpm under full load condition. The L_d and L_q corresponding to the RMS current of 2.5A are set to 0.0449H and 0.1051H, respectively in the IPMSM model. It is clear that with the same current level as shown in the top graph (ia), the current derivatives at two active-voltage vectors estimated

by experiment match closely with those obtained by simulation. The experimental phase currents of the IPMSM were filtered by using the RC filter with the cut-off frequency of 100 kHz.

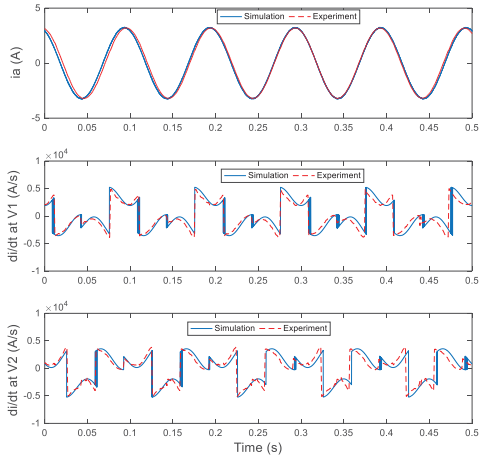

Fig. 4. Derivatives of motor currents at the first and second active-voltage vectors during each PWM cycle under full load at speed of 300 rpm.

B. Experimental results of the proposed sensorless control method

Comparative studies on the estimation accuracy between the proposed sensorless method and the conventional FPE sensorless method, which employs the current derivatives at two active-and two zero-voltage vectors were conducted at low speeds. Fig. 5(a) and Fig. 5(b) present the performance of the proposed sensorless method and the conventional FPE sensorless method at 30 rpm (1Hz) under full load, respectively. It is clear that the position error of the proposed sensorless method is within 7 electrical degrees, which is much smaller than the position error (within 20 electrical degrees) of the conventional FPE sensorless method.

A comparative study of the current distortion caused by the pulse extension of the proposed sensorless method and the conventional FPE sensorless method was implemented with the same t_{min} (16 μs). Total Harmonic Distortions (THD) at different speeds under full-load condition is presented in Fig. 6. It is clear that the proposed sensorless method causes a smaller current distortion over the whole speed range. The THDs of the stator current with the proposed method are less than 2.9% in all tested conditions. The THD of the conventional FPE sensorless method is about 30% higher than that of the proposed sensorless method in low speed range. In medium and high speed ranges (over 600 rpm), the current is significantly distorted by the conventional FPE sensorless method with the THDs about double of those caused by the proposed method. The THD caused by the conventional FPE sensorless method increases when the speed and load increases, reaching about 5.57% at the rated speed of 1500 rpm under full load.

C. Experimental result of the proposed on-line parameter identification method

Fig. 7 compares the inductances estimated by the proposed on-line method and the inductances measured by using the AC standstill off-line method shown in [19]. The IPMSM is operated at 500 rpm and load current is adjusted from 0.25A (no load) to 3A (approx 120% of rated load). It is clear that the estimated inductances are almost the same as the off-line measured ones.

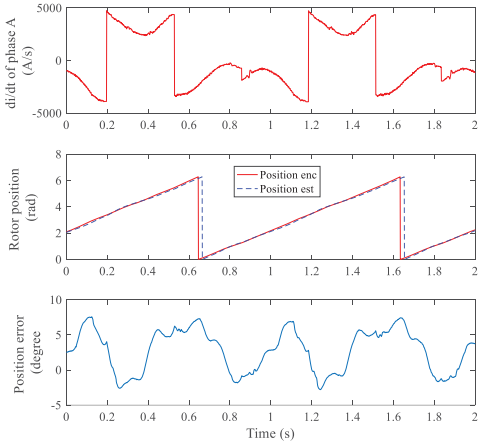

(a) Proposed sensorless method.

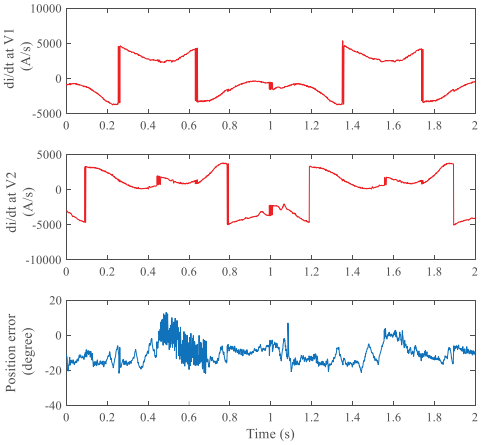

(b) Conventional FPE sensorless method.

Fig. 5. Comparative study of two sensorless methods at 30 rpm under full load (experiment).

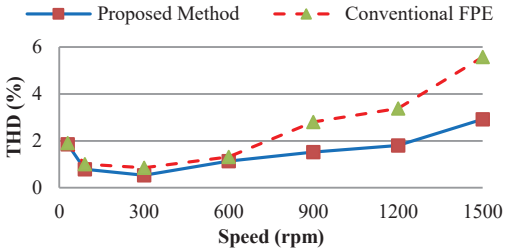

Fig. 6. Total Harmonic Distortion under full load.

The experimental results of the proposed method when the machine accelerates from zero to 900 rpm are presented in Fig. 8. When the machine starts accelarating from 1.05s, the stator RMS current abruptly rises from 0.9A to 2.6 A. The estimated L_q abruptly drops from about 138 mH to 110mH. During this period, the estimated L_d increases slightly by about 1 mH from 45 mH. After the acceleration is over, the RMS stator current falls to 1A, and the estimated L_q returns back to about 137 mH. The estimated L_d remaines almost unchanged after the torque transient, as is also expected. Clearly, the proposed on-

line method tracks the variation of inductances with variation of stator RMS current during the transient state close to the inductances found from off-line tests.

Results presented in Fig. 8 have also shown that the proposed method estimate the dq inductances very fast (within a PWM period) and that the inductances can be estimated at zero speed and during transients.

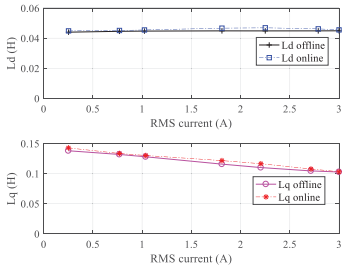

Fig. 7. Online estimation of inductances at 500 rpm (experiment).

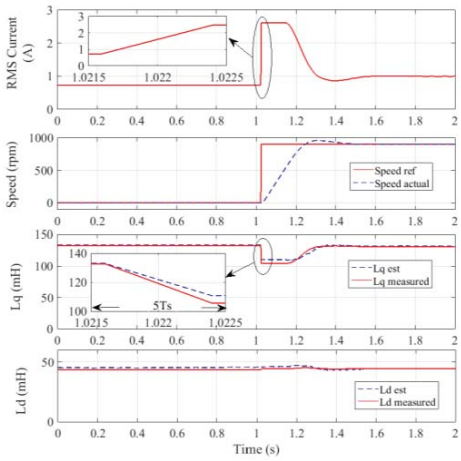

Fig. 8. Estimated inductances versus RMS current during the acceleration from zero to 900 rpm (experiment).

V. Conclusion

This paper has shown that the rotor speed and position can be estimated satisfactorily over a full speed range from zero to rated speed based on the measurement of current derivatives at one active- voltage vector and one zero-voltage vector during each PWM cycle. The effect of common-mode noise on current derivative measurement has been addressed. With the proposed sensorless method, the estimation accuracy is improved at low speeds and total harmonic distortion is reduced over a full speed range, compared to the conventional FPE sensorless method. In addition, the variation of machine inductances with load variation can be tracked on-line every PWM cycle by measuring current derivatives and the DC bus of the inverter during each PWM cycle. The high estimation accuracy of the proposed on-line method during steady and fast transient states was verified by comparing the estimated inductances with the values measured off-line.

References

[1] M. Schrodl and M. Lambeck, "Statistic properties of the INFORM method for highly dynamic sensorless control of PM motors down to standstill," in *Industrial Electronics Society, 2003. IECON '03. The 29th Annual Conference of the IEEE*, 2003, pp. 1479-1486 Vol.2.

[2] J. Holtz and J. Juliet, "Sensorless acquisition of the rotor position angle of induction motors with arbitrary stator windings," *IEEE Transactions on Industry Applications,* vol. 41, pp. 1675-1682, 2005.

[3] Y. Hua, M. Sumner, G. Asher, Q. Gao, and K. Saleh, "Improved sensorless control of a permanent magnet machine using fundamental pulse width modulation excitation," *IET Electric Power Applications,* vol. 5, pp. 359-370, 2011.

[4] Q. Gao, G. M. Asher, M. Sumner, and P. Makys, "Position Estimation of AC Machines Over a Wide Frequency Range Based on Space Vector PWM Excitation," *IEEE Transactions on Industry Applications,* vol. 43, pp. 1001-1011, 2007.

[5] M. A. Vogelsberger, S. Grubic, T. G. Habetler, and T. M. Wolbank, "Using PWM-Induced Transient Excitation and Advanced Signal Processing for Zero-Speed Sensorless Control of AC Machines," *IEEE Transactions on Industrial Electronics,* vol. 57, pp. 365-374, 2010.

[6] S. Bolognani, S. Calligaro, R. Petrella, and M. Sterpellone, "Sensorless control for IPMSM using PWM excitation: Analytical developments and implementation issues," in *2011 Symposium on Sensorless Control for Electrical Drives*, 2011, pp. 64-73.

[7] D. Q. Guan, D. Xiao, and M. F. Rahman, "Comparison of torque control bandwidth of HF injection, SMO and FPE Direct Torque control IPMSMS drives," in *2014 Australasian Universities Power Engineering Conference (AUPEC)*, 2014, pp. 1-6.

[8] "IEEE Standard Procedures for Obtaining Synchronous Machine Parameters by Standstill Frequency Response Testing (Supplement to ANSI/IEEE Std 115-1983, IEEE Guide: Test Procedures for Synchronous Machines)," *IEEE Std 115A-1987,* p. 0_1, 1987.

[9] T. L. Vandoorn, F. M. D. Belie, T. J. Vyncke, J. A. Melkebeek, and P. Lataire, "Generation of Multisinusoidal Test Signals for the Identification of Synchronous-Machine Parameters by Using a Voltage-Source Inverter," *IEEE Transactions on Industrial Electronics,* vol. 57, pp. 430-439, 2010.

[10] E. C. Bortoni and J. A. Jardini, "A standstill frequency response method for large salient pole synchronous machines," *IEEE Transactions on Energy Conversion,* vol. 19, pp. 687-691, 2004.

[11] S. A. Odhano, P. Giangrande, R. I. Bojoi, and C. Gerada, "Self-Commissioning of Interior Permanent- Magnet Synchronous Motor Drives With High-Frequency Current Injection," *IEEE Transactions on Industry Applications,* vol. 50, pp. 3295-3303, 2014.

[12] D. Q. Dang, M. S. Rafaq, H. H. Choi, and J. W. Jung, "Online Parameter Estimation Technique for Adaptive Control Applications of Interior PM Synchronous Motor Drives," *IEEE Transactions on Industrial Electronics,* vol. 63, pp. 1438-1449, 2016.

[13] K. Liu, Q. Zhang, J. Chen, Z. Q. Zhu, and J. Zhang, "Online Multiparameter Estimation of Nonsalient-Pole PM Synchronous Machines With Temperature Variation Tracking," *IEEE Transactions on Industrial Electronics,* vol. 58, pp. 1776-1788, 2011.

[14] M. S. Rafaq, F. Mwasilu, J. Kim, H. H. Choi, and J. W. Jung, "Online Parameter Identification for Model-Based Sensorless Control of Interior Permanent Magnet Synchronous Machine," *IEEE Transactions on Power Electronics,* vol. 32, pp. 4631-4643, 2017.

[15] M. X. Bui, D. Xiao, M. F. Rahman, and D. Q. Guan, "Online estimation of inductances of permanent magnet synchronous machines based on current derivative measurements," in *20th International Conference on Electrical Machines and Systems (ICEMS)*, Sydney, Australia, 2017, pp. 1-6.

[16] A. Piippo, M. Hinkkanen, and J. Luomi, "Analysis of an adaptive observer for sensorless control of interior permanent magnet synchronous motors," *IEEE Transactions on Industrial Electronics,* vol. 55, pp. 570-576, Feb 2008.

[17] G. Narayanan, D. Zhao, H. K. Krishnamurthy, R. Ayyanar, and V. T. Ranganathan, "Space Vector Based Hybrid PWM Techniques for Reduced Current Ripple," *IEEE Transactions on Industrial Electronics,* vol. 55, pp. 1614-1627, 2008.

[18] D. Q. Guan, D. Xiao, M. X. Bui, and M. F. Rahman, "Current derivative estimation by using AMR current sensor and its application in sensorless control of an IPMSM drive," in *2017 IEEE Energy Conversion Congress and Exposition (ECCE)*, Ohio, USA, 2017, pp. 1901-1908.

[19] R. Dutta and M. F. Rahman, "A comparative analysis of two test methods of measuring d- and q-axes inductances of interior permanent-magnet machine," *IEEE Transactions on Magnetics,* vol. 42, pp. 3712-3718, Nov 2006.